J|A|C|S
ARTICLES
Published on Web 03/17/2006

Electron Transfer from Sodium to Oriented Nitromethane, CH_3NO_2: Probing the Spatial Extent of Unoccupied Orbitals

Philip R. Brooks,* Peter W. Harland,† and Crystal E. Redden

Contribution from the Chemistry Department and Rice Quantum Institute, Rice University, Houston, Texas 77001

Received December 2, 2005; E-mail: brooks@python.rice.edu

Abstract: Beams of sodium atoms with energies of a few eV are crossed with a beam of oriented CH_3NO_2 molecules to study the effect of collision energy and orientation on electron transfer. The electron transfer produces Na^+ ions and free electrons, parent negative ions ($CH_3NO_2^-$), and fragmentation ions NO_2^- and O^- in proportions that depend on the collision energy. The steric asymmetry is very small or zero and suggests that production of all of the ions is favored by sideways attack with respect to the permanent dipole along the C−N axis. In these experiments, the electron appears to be transferred into the $^2B_1$ state of the anion comprising mainly the π^*_{NO} LUMO, producing a valence-bound state rather than a dipole-bound state.

I. Introduction

Nitromethane is a fascinating molecule. It is one of the simplest nitrogen-containing molecules, is a prototype explosive,[1] and perhaps plays a role in the atmosphere.[2] The NO_2 group behaves as a halogen, and the reactivity of CH_3NO_2 with alkali metals was originally[3] conjectured to be similar to that of CH_3I, the standard of molecular reaction dynamics. Despite rough similarities in the strengths of the bonds to be broken and made in the two cases, important differences were observed arising from the different electronic structures in the two molecules.[3−5]

The halogen-like behavior of the NO_2 group suggested that reaction proceeds via an electron-transfer mechanism. Photodissociation has probed unoccupied states of the neutral molecule,[6−9] and electron transfer from different donors (alkali metal atoms,[10−13] high Rydberg atoms,[13−16] and free electrons[14,17−19]) has probed various aspects of the (transient) $CH_3NO_2^-$ anion. There is general agreement that the LUMO is the π^*_{NO} orbital and that several low-lying states of the anion may be accessed in the various experiments. The parent anion, $CH_3NO_2^-$, is a stable valence-bound anion with an adiabatic electron affinity of 0.26 eV.[13] The electron can apparently also be weakly bound (∼12 meV) in the field of the very strong dipole moment (3.46 D)[20] to form a dipole-bound state (DBS), and calculations[21] show that this DBS lies very close in energy to the neutral. This DBS has been postulated to be a doorway state[13] whereby the electron is initially captured into a diffuse dipole-bound orbital at the CH_3 end of the molecule followed by a geometrical rearrangement to give the valence-bound state (VBS).

The steric requirements for forming the two different states are likely to be different. The dipole-bound anion is formed in an almost resonant process from weakly bound high Rydberg atoms to give an anion in which the electrons are bound at the positive (CH_3) end of the dipole. On the other hand, thermal collisions in crossed beams produced MNO_2 in roughly equal amounts in the forward and backward hemisphere, consistent with broadside attack of the alkali metal at the nitrogen moiety. Salt formation thus seems not to require the DBS as a precursor. These apparently contradictory observations might be reconciled if attack at different ends of the molecule produced different ions.

† Present address: Chemistry Department, University of Canterbury, Christchurch, New Zealand.

(1) Gruzdkov, Y. A.; Gupta, Y. M. *J. Phys. Chem.* **1998**, *102*, 8325−8332.
(2) Taylor, W. D.; Allston, T. D.; Moscato, M. J.; Fazekas, G. B.; Kozlowski, R.; Takacs, G. A. *Int. J. Chem. Kinetics* **1980**, *12*, 231−240.
(3) Herm, R. R.; Herschbach, D. R. *J. Chem. Phys.* **1970**, *52*, 5783−5792.
(4) Parrish, D. D.; Herm, R. R. *J. Chem. Phys.* **1971**, *54*, 2518−2528.
(5) Sholeen, C. M.; Herm, R. R. *J. Chem. Phys.* **1976**, *65*, 5398−5407.
(6) Butler, L. J.; Krajnovich, D.; Lee, Y. T.; Ondrey, G.; Bersohn, R. *J. Chem. Phys.* **1983**, *79*, 1708−1715.
(7) Blais, N. C. *J. Chem. Phys* **1983**, *79*, 1723−1729.
(8) Wodtke, A. M.; Hintsa, E. J.; Lee, Y. T. *J. Chem. Phys.* **1986**, *84*, 1044.
(9) Wodtke, A. M.; Hintsa, E. J.; Lee, Y. T. *J. Phys. Chem.* **1986**, *90*, 3549−3558.
(10) Compton, R. N.; Reinhardt, P. W.; Cooper, C. D. *J. Chem. Phys.* **1978**, *68*, 4360−4367.
(11) Fluendy, M. A. D.; Lunt, S. *Mol. Phys.* **1983**, *49*, 1007−1016.
(12) Lobo, R. F. M.; Moutinho, A. M. C.; Lacmann, K.; Los, J. *J. Chem. Phys.* **1991**, *95*, 166−175.
(13) Compton, R. N.; Carman, H. S., Jr.; Desfrançois, C.; Abdoul-Carmine, H.; Schermann, J. P.; Hendricks, J. H.; Lyapustina, S. A.; Bowen, K. H. *J. Chem. Phys.* **1996**, *105*, 3472−3478.
(14) Stockdale, J. A.; Davis, F. J.; Compton, R. N.; Klots, C. E. *J. Chem. Phys.* **1974**, *60*, 4279.
(15) Lecomte, F.; Carles, S.; Desfrançois, C.; Johnson, M. A. *J. Chem. Phys.* **2000**, *113*, 10973−10977.
(16) Suess, L.; Parthasarathy, R.; Dunning, F. B. *J. Chem. Phys.* **2003**, *119*, 9532−9537.
(17) Flicker, W. M.; Mosher, O. A.; Kuppermann, A. *Chem. Phys. Lett.* **1979**, *60*, 518−522.
(18) Walker, I. C.; Fluendy, M. A. D. *Int. J. Mass Spectrom.* **2001**, *205*, 171−182.
(19) Sailer, W.; Pelc, A.; Matejcik, S.; Illenberger, E.; Scheier, P.; Märk, T. D. *J. Chem. Phys.* **2002**, *117*, 7989−7994.
(20) Nelson, R. D. J.; Lide, D. R. J.; Maryott, A. A. *Natl. Stand. Ref. Ser. - Natl. Bur. Stand.* **1967**, *10*.
(21) Gutsev, G. L.; Bartlett, R. J. *J. Chem. Phys.* **1996**, *105*, 8785−8792.

The present experiments have thus explored the energetic and steric requirements for producing different negative ions by colliding beams of fast sodium atoms with beams of CH_3NO_2 molecules that are state-selected and oriented before the collision. Different negative ions are formed, depending on the energy, but the steric asymmetry is very small or zero, consistent with their formation by broadside attack. There is no steric evidence to suggest that a precursor to the stable $CH_3NO_2^-$ ion is formed by attack at the CH_3-end of the molecule, and thus, the processes observed here apparently do not involve the DBS.

II. Experimental Section

The apparatus has been discussed in several earlier papers.[22−25] Briefly, liquid CH_3NO_2 is contained in a cylinder held at 0 °C giving a vapor pressure of about 21 Torr. Helium is blown through the cylinder into the supersonic nozzle to give a final total pressure of ∼150 Torr. A fiberglass wick is immersed in the liquid in the cylinder to provide a large surface area for evaporation. The seeded beam passes through a skimmer and a second aperture before entering a 1.4 m electric hexapole deflection field. The hexapole does not contain any beam stops, so a weak beam is transmitted even if no voltage is applied to the rods. When high voltage (HV) is applied (typically ±10 kV on 6.35 mm rods) molecules such as CH_3NO_2 with first-order Stark effects are focused toward the axis, and the beam intensity increases. The beam leaving the hexapole passes through an ultrahigh vacuum (uhv) chamber, ultimately being dumped into a chamber pumped with a 140 L/s ion pump.

Fast sodium atoms are generated in a single chamber oven where the atoms are surface ionized on a Re wire. The wire is biased 5−30 V positive with respect to ground, and the positive ions are accelerated toward a grounded slit about 0.5 mm from the filament. The resulting ions are resonantly charge-exchanged by residual sodium atoms before leaving the oven. A beam of fast neutrals emerges from the oven, and any ions are removed from the beam by an electric deflecting field. This beam also passes through the uhv chamber, intersecting the gas beam at right angles between two time-of-flight (TOF) mass spectrometers.

The hexapole field focuses molecules that are in low-field-seeking states. These focused molecules pass into the uhv chamber where they are oriented in the uniform electric field between the two TOF mass spectrometers, with the positive (CH_3) end of the dipole pointing toward the mass spectrometer that is positively charged. The molecules experience a weak electric field between the hexapole and the reaction zone to ensure that the selected states do not randomize by nonadiabatic processes.[26,27] Even though CH_3NO_2 is an asymmetric top, the barrier to internal rotation about the C−N bond is extremely low (2.11 cm^{-1}),[28] and the NO_2 group spins freely about the CN bond so that CH_3NO_2 behaves as a symmetric top.[29] The hexapole state-selection process and adiabatic transition to a uniform field thus produces CH_3NO_2 molecules which are oriented with the CH_3-group toward the incoming Na atom or with the NO_2-group toward the incoming Na atom, depending on the polarity of the TOF mass spectrometers.

Electron transfer between neutral species produces a positive ion and a negative ion that can be separated if the energy exceeds the threshold for ion pair formation. These ions are each accelerated to separate TOF mass spectrometers and detected by separate microchannel plate (MCP) detectors. The TOF voltages are dc, and the beams are continuous, and thus there is no time zero for the mass spectrometers. Since the ions are made simultaneously, the *difference* in flight time is a signature of the mass of the negative ion, assuming that the positive ion is Na^+. The pulse from the positive ion starts a time-to-digital converter (TDC); the pulse from the negative ion is delayed 4 μs (to be sure that the positive ion pulse always arrives first), and stops the TDC.

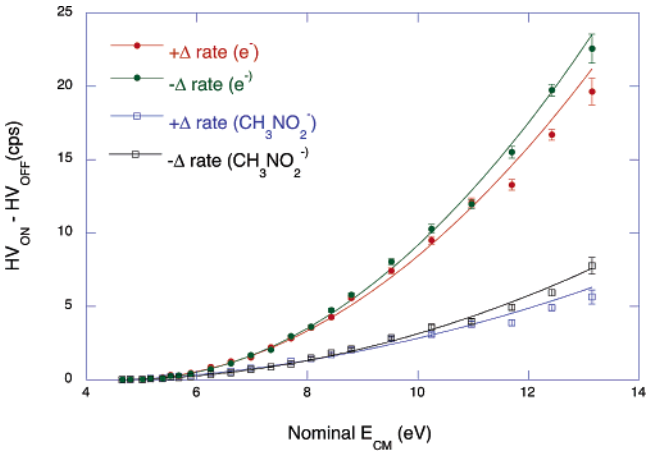

Figure 1. Representative $HV_{ON}-HV_{OFF}$ signals (ΔHV) plotted vs the nominal CM energy. Curves are fit with a quadratic threshold function to give apparent thresholds of ∼3.8 eV (m/e = 61) and ∼4.6 eV (m/e = 0). Signals for attack at positive or negative end are denoted +Δ or −Δ.

III. Results

3.1. Mass Spectra. Electron transfer clearly produces Na^+, and several different negative ions, depending on the energy available to the system. Electrons, parent negative ions ($CH_3NO_2^-$), and the fragment ions, O^- and NO_2^-, are all formed from CH_3NO_2. Small negative ion signals are observed at m/e = 26 (CN^-), 32 (O_2), and 122 $(CH_3NO_2)_2^-$, but these are *not* affected by the HV and are therefore *not* from CH_3NO_2. We believe that signals at m/e = 32 are from a leak in the gas-handling system, and those at m/e = 26 and 122 are from CH_3NO_2 dimers. In addition small signals are produced at m/e = 42 (CNO^-) which *is* affected by the HV and apparently arises from CH_3NO_2. Signals at m/e = 26, 42, and 122 were too weak to analyze further.

3.2. Energy Calibration. The nominal laboratory energy is the voltage applied to the surface ionizing filament, but the voltage drop along the filament and various contact potentials in the oven require calibration of the energy scale. Even though these experiments are designed to measure steric effects and *not* ion pair thresholds, *apparent* thresholds are determined for each ion by plotting signal vs nominal CM energies calculated from the nominal laboratory energy, as in Figure 1. (Figure 1 compares raw signals for positive and negative attack and conclusions about which end is more reactive requires information about detector sensitivity, which is obtained by equating signals with HV_{OFF}.[24])

Quadratic curves were fit to the data above threshold:

$$\sigma = 0 \ (E < Th)$$

$$\sigma = a(E - Th)^2 \ (E \geq Th)$$

The constant, a, is a scale factor which varies from day to day, and for this reason the thresholds were determined for each day's data. In all cases, the apparent threshold for forming the parent

(22) Harris, S. A.; Wiediger, S. D.; Brooks, P. R. *J. Phys. Chem.* **1999**, *103*, 10035−10041.
(23) Harris, S. A.; Harland, P. W.; Brooks, P. R. *Phys. Chem. Chem. Phys.* **2000**, *2*, 787−791.
(24) Brooks, P. R.; Harris, S. A. *J. Chem. Phys.* **2002**, *117*, 4220−4232.
(25) Harland, P. W.; Brooks, P. R. *J. Am. Chem. Soc.* **2003**, *125*, 13191−13197.
(26) Brooks, P. R.; Jones, E. M.; Smith, K. *J. Chem. Phys.* **1969**, *51*, 3073.
(27) Brooks, P. R. *Faraday Discuss. Chem. Soc.* **1973**, *55*, 299−306.
(28) Lin, C. C.; Swalen, J. D. *Rev. Mod. Phys.* **1959**, *31*, 841−892.
(29) Jones, E. M.; Brooks, P. R. *J. Chem. Phys.* **1970**, *53*, 55.

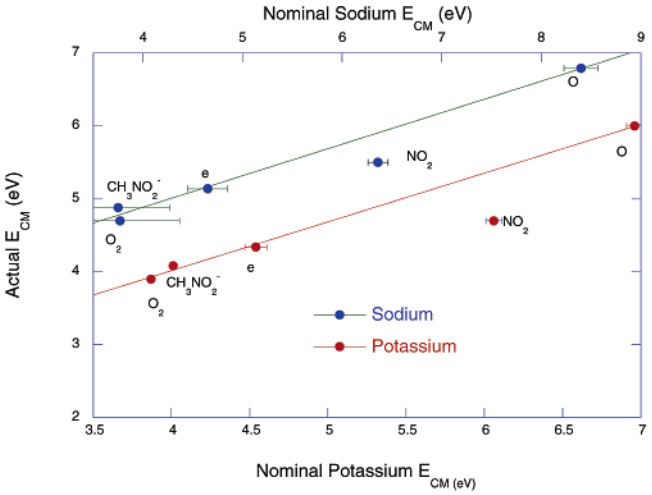

Figure 2. Actual (literature) threshold values for various ions plotted vs "nominal" threshold energies determined here. Lines are least-squares fits to the points excluding the NO_2^- signals.

negative ion, $CH_3NO_2^-$, was lower than the threshold for forming the electron, e^-, showing that the parent negative ion is stable with respect to autodetachment. The energy calibration (Figure 2) depends on the beam source conditions.

The hexapole field focuses molecules that have first-order Stark effects, and the CH_3NO_2 beam intensity increases when HV is applied to the hexapole field. The difference between the signal with the HV on and off (ΔHV signal) is positive, as shown in Figure 1, and thus represents signal from oriented molecules. For e^-, O^-, NO_2^-, and $CH_3NO_2^-$, thresholds were evaluated using ΔHV signals, as well as the raw signal with HV on (HV_{ON}), which could include contributions from background or from small concentrations of dimer. The thresholds did not depend on orientation or on whether the difference signals were used. Since the absolute signal rate (plotted in Figure 1) depends on the beam intensities, which differ from day to day, the final nominal thresholds were the averages of thresholds determined for each separate run. The energy was calibrated by plotting in Figure 2 our "nominal" threshold energy for each ion vs the actual threshold energy calculated from literature values shown in Table 1. The O_2^- threshold was determined from the HV_{ON} signals because the focusing voltage does not affect O_2^-.

Since the threshold for NO_2^- seemed to be systematically different from the calibration obtained using the other ions, a similar plot was made using preliminary data for production of these ions from potassium. In both cases, the experimental threshold for formation of NO_2^- lies higher (0.6 eV for K and 0.4 eV for Na) than expected from values calculated from bond dissociation energies, suggesting that there may be an activation energy for the formation of NO_2^-.

3.3. Steric Asymmetry. The steric asymmetry factor is defined as

$$G = \frac{\sigma_- - \sigma_+}{\sigma_- + \sigma_+}$$

where $\sigma_\pm$ is the cross section for positive- (or negative)-end approach. Experimental values of G are calculated by comparing values of $\Delta HV/HV_{OFF}$ for positive-end and negative-end orientation, where HV_{OFF} are signals from *randomly* oriented molecules with no HV applied to the focusing field.[24] Figures 3−6 show the steric asymmetry for forming various negative ions as a function of energy above the ionization potential of the alkali atom. The energy is determined from the calibration in Figure 2.

Table 1. Thermodynamic Values (eV)

species/bond	EA	IP	BDE	ref	species/bond	EA	IP	BDE	ref
Na		5.14		30	NO_2	2.27			30
K		4.34		30	CH_3NO_2	0.26			13
O	1.46			30	C−N			2.64	31
O_2	0.45			30	NO−O			3.11	32

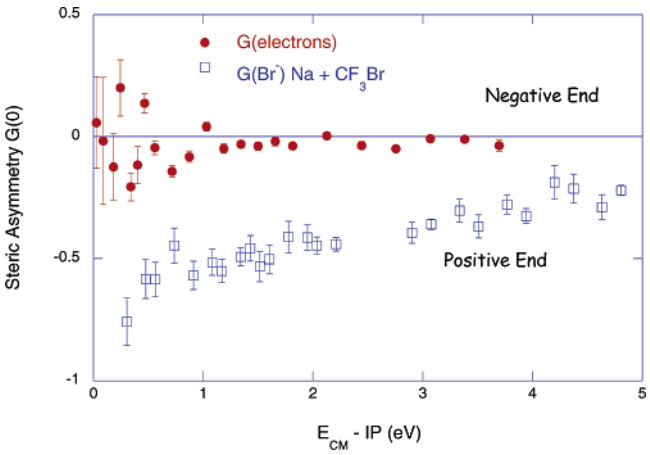

Figure 3. Steric asymmetry for electrons. For comparison, open squares are steric asymmetry factors for formation of Br^- from Na + CF_3Br.

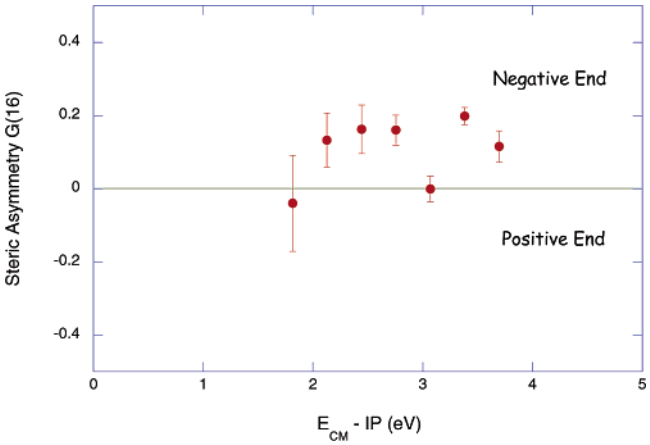

Figure 4. Steric asymmetry for formation of O^-.

The steric asymmetry is essentially zero for all of the ions produced, although tantalizing deviations from zero are sometimes apparent. The apparent insensitivity to orientation could arise if the orientation of the CH_3NO_2 molecules were scrambled by nonadiabatic transitions in the region between the hexapole field and the reaction zone.[26,27] This has been previously avoided by maintaining a weak electric field in the region between the hexapole and the reaction zone. To rule out nonadiabatic transitions in these experiments, several test measurements (not shown here) were made on mixtures of CF_3Br and CH_3NO_2, and in every case the steric asymmetry factor of CH_3NO_2 was near zero, but that for CF_3Br was not. (The steric asymmetry factor[25] for Na reacting with CF_3Br to form Br^- is shown in Figure 3 for illustration.) This shows that CF_3Br makes adiabatic

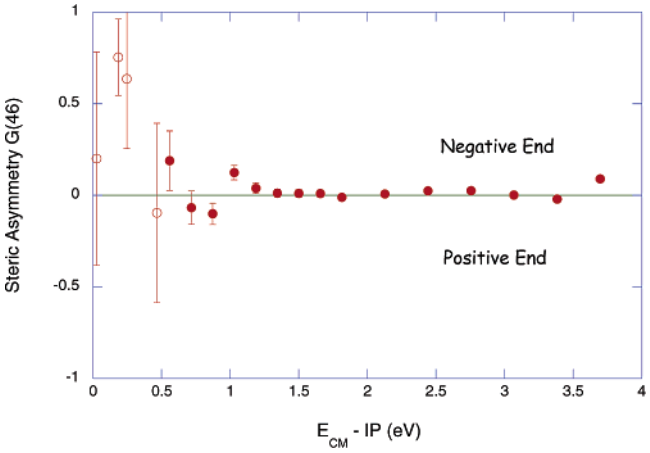

Figure 5. Steric asymmetry for formation of NO_2^-. Open symbols are data taken at energies below "threshold".

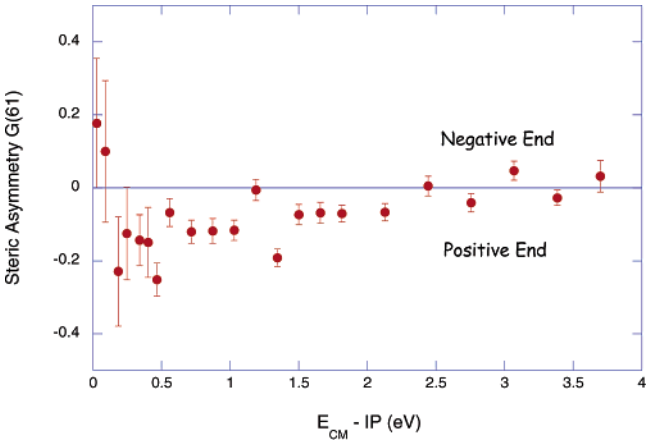

Figure 6. Steric asymmetry for formation of parent negative ion, $CH_3NO_2^-$.

transitions between the state-selecting hexapole field and the reaction zone, and it is reasonable to conclude that CH_3NO_2 does, too.

Even though the steric asymmetry is very small, Figure 3 suggests that electron formation might be favored very weakly by CH_3-end attack. The steric asymmetry of NO_2^- seems to be zero, and the formation of $CH_3NO_2^-$ is weakly favored by CH_3-end attack. Figure 4 suggests that O^- is weakly favored by NO_2-end attack. We have been unable to identify any strong trends in the steric asymmetry. The preliminary experiments with potassium show similar steric asymmetry, suggesting that any "tantalizing deviations" are probably not real. We believe that the steric asymmetry suggests that sideways attack is most favorable. [The steric asymmetry results from four separate measurements (HV on and off for positive and negative orientation), and the sign is particularly sensitive to fluctuations in small signals.]

3.4. Ion Fractions. The fraction of ions formed as a function of energy is shown in Figures 7 and 8. Because the steric asymmetry for the NO_2^- ions appears to be zero, its fraction is independent of the attack geometry, and only positive-end attack signals are shown in Figure 7.

The sodium data clearly indicate that the maximum fraction of electrons produced is about 1 eV above the ionization potential of sodium. Electron attachment apparently produces (transient) negative ions; some live long enough ($>\sim 3\ \mu$s, the transit time of Na^+ in the TOF) to be detected as the parent

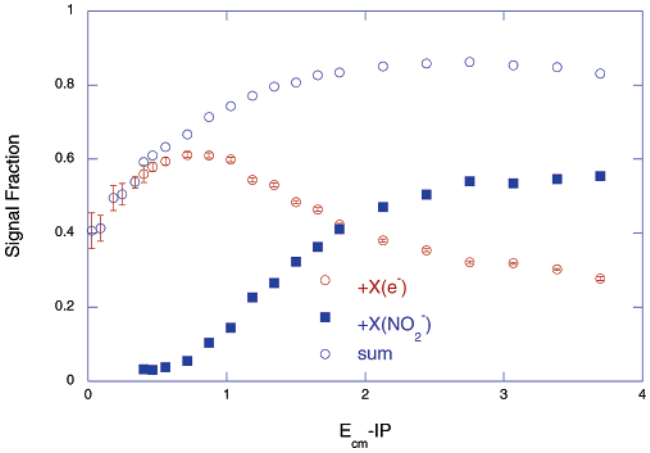

Figure 7. Signal fractions of electrons (open circles) and NO_2^- ions (squares) vs energy above IP for positive end attack. (Negative end attack fractions are virtually identical and are omitted for clarity.) Open blue circles are fractions due to the sum of electrons and NO_2^- ions.

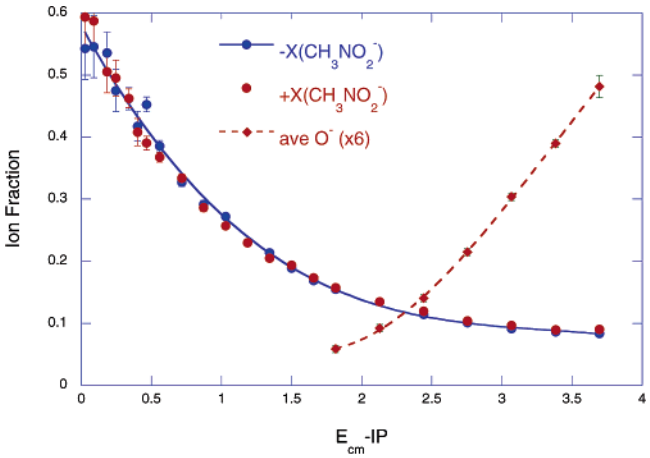

Figure 8. Fraction of ion signal from $CH_3NO_2^-$ for positive end and negative end attack and average fraction of O^-. Lines are cubic fits to guide the eye.

negative ion, $CH_3NO_2^-$, and others autodetach the electron on a time scale $\ll 3\ \mu$s. The lifetime estimates are based on the absence of any broadening of the mass peaks in the mass spectrum. At energies beyond the threshold to break the C−N bond (~0.5 eV) the transient negative ion preferentially fragments to form NO_2^-, again on a time scale $\ll 3\ \mu$s.

Calculations

Gaussian calculations were performed to investigate the qualitative geometry of the low-lying molecular orbitals. The equilibrium ground-state geometry of the neutral was optimized at the MP2 level of theory using the aug-cc-pvtz basis set.[33] Full Mulliken population analyses were carried out for the *neutral* in this geometry and for the anion geometry determined by Gutsev and Bartlett[21] where the plane of the NO_2 group is tilted from the C−N axis ~34°. As shown in Figure 9a and 9b, the HOMO in both geometries is a π orbital centered on the NO_2 moiety. The LUMO for the neutral geometry, Figure 9c, is a large Rydberg-type orbital at the CH_3 end as might be expected for a dipole-bound state. The nature of this orbital is very sensitive to the tilt angle,

(30) *NIST*; NIST Standard Reference Database Number 69; 2003.
(31) McMillen, D. F.; Golden, D. M. *Annu. Rev. Phys. Chem.* **1982**, *33*, 493−532.
(32) Radzig, A. A.; Smirnov, B. M. *Reference Data on Atoms, Molecules, and Ions*; Springer: Berlin, 1985.
(33) Frisch, M. J.; et al. Gaussian, Inc.: Wallingford, CT, 2004.

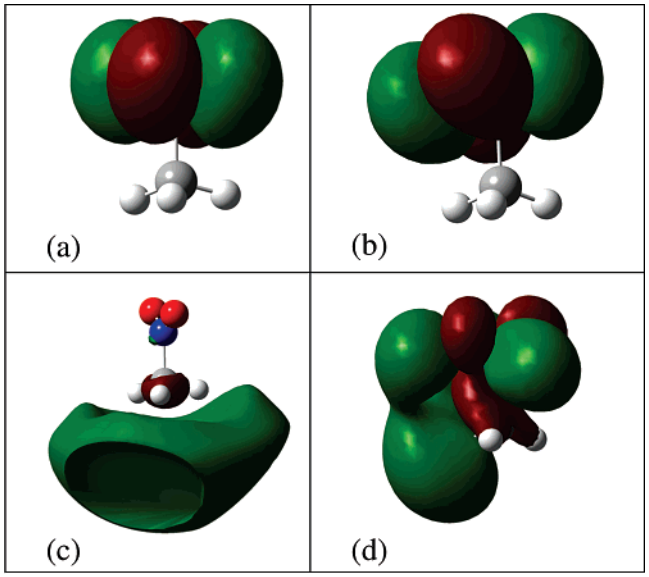

Figure 9. Gaussian orbitals. (a) HOMO for neutral CH_3NO_2; (b) HOMO for neutral CH_3NO_2 in the bent geometry of the anion; (c) LUMO for neutral CH_3NO_2; (d) LUMO for neutral CH_3NO_2 in the bent geometry of the anion.

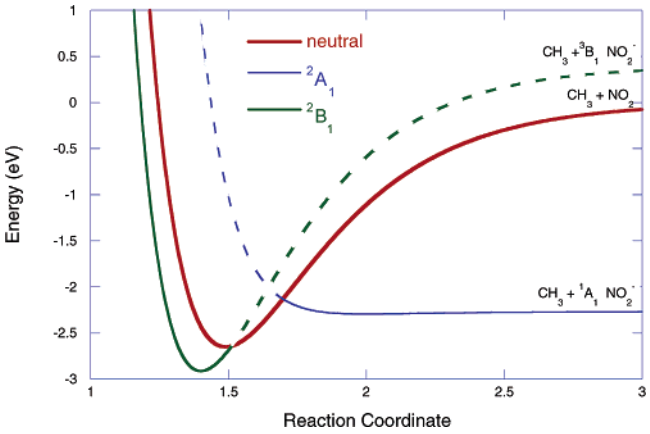

Figure 10. Schematic potential energy curves for neutral ground-state CH_3NO_2 and the two lowest-lying anion states, $^2B_1$ (π^*), and $^2A_1$(σ^*). The reaction coordinate is the C−N distance at large energies but includes different anion geometries at small distances. Dashed portions of the anion curves indicate regions where the anion is unstable with respect to the neutral molecule plus an electron.

and as shown in Figure 9d the LUMO in the bent anion geometry is *not* the Rydberg-type of orbital, but rather a complex π^*-type orbital at the NO_2 end extending toward the hydrogens. Similar calculations for the *anion* show that the HOMO (the orbital now accommodating the extra electron) resembles Figure 9d in either geometry.

IV. Discussion

Walker and Fluendy[18] have recently studied the optical spectra and electron energy loss spectra of CH_3NO_2 and have summarized the existing data in a coherent discussion of the anionic states of nitromethane. We will augment their discussion with the results obtained in the present experiments.

Figure 10, adapted from their paper, represents schematic potential energy curves for the neutral molecule and two low-lying anion states, $^2B_1$ and $^2A_1$. (The spectroscopy of CH_3NO_2 is usually discussed in C_{2v} symmetry because the electron density is concentrated at the NO_2 end of the molecule.) Experiment and calculation agree that the LUMO is the $^2B_1$ orbital corresponding to occupation of the π^*_{NO} orbital; the adiabatic electron affinity is 0.26 eV.[13] The anion geometry is *different* from that of the neutral: the N is closer to tetrahedral, with the plane of the $NO_2 \approx 34°$ from the C−N axis.[21] The C−N bond in the anion is a bit shorter than that in the neutral, whereas the N−O bond is somewhat larger, consistent with occupation of the π^*_{NO} orbital. The curve representing the $^2B_1$ state thus represents a different geometry than the curve for the neutral, and this state must correlate with a B state of NO_2^- (probably $^3B_1$).[34]

The $^2A_1$ state of $CH_3NO_2^-$ correlates with the ground $^1A_1$ state of NO_2^- but this state lies above the neutral molecule and has a *negative* electron affinity.

The lowest energies in the present experiments produce only the parent negative ion, $CH_3NO_2^-$. These energies are so low as to *require* that the electron be transferred to the LUMO, which in our experiments is the π^*_{NO} orbital because the incoming Na^+ ion changes the geometry of the molecule. The steric asymmetry for formation of the parent negative ion, $CH_3NO_2^-$, is small, and attack at the CH_3-end is only slightly favored at low energies. This steric asymmetry is so small that it seems likely to be a consequence of salt production[3−5] rather than a signature of a dipole-bound state. Formation of $NaNO_2$ (by recombination of ions) will be favored if the Na^+ ion is near the NO_2 end of the molecule regardless of the electron-transfer event. The salt is not detected in the present experiments, but its formation would reduce the ion signal from NO_2-end attack, leaving a slight preference for CH_3-end attack.

Increasing the energy is likely to populate higher vibrational levels of the $^2B_1$ state. These states can lie in the continuum of the neutral molecule plus free electron, and thus autodetach to produce free electrons, illustrated by using dashed lines for those portions of the ionic curves lying above the neutral molecule. The steric asymmetry for formation of the free electron appears to be zero, suggesting that salt formation is not competitive with electron ejection. Electron transfer to the π^*_{NO} $^2B_1$ state is not expected to affect the C−N bonding, and the state is expected to be stable as shown.

The C−N bond can be broken, giving $NaNO_2$ in thermal experiments[3−5] and NO_2^- at higher energies,[12,13] and the $^2A_1$ state must be involved, either by direct electron transfer or by internal conversion from the $^2B_1$ state. As suggested in Figure 10, attachment of *free* electrons to produce the $^2A_1$ state via a vertical Franck−Condon transition would be favored at energies ~2 eV.[18] Such a vertical transition produces the $^2A_1$ state again in the continuum, and electron ejection is expected to be more rapid than nuclear rearrangement to break the C−N bond. Thus, the more likely scenario for C−N bond cleavage is that free electrons attach to form the $^2B_1$ state at lower energy (~0.7 eV[18]), followed by a curve crossing to the $^2A_1$ state in a configuration where bond breaking is more likely.

Free electrons attach to neutral molecules in a vertical (Franck−Condon) process, leaving the nuclear positions unchanged, and Rydberg electrons approximate free electrons,[35] especially for high principal quantum numbers.[36] In contrast, electron transfer from alkali metal atoms as in the present experiments involves a curve crossing where the Born−

(34) Cai, Z.-L. *J. Chem. Soc., Faraday Trans.* **1993**, *89*, 991−994.
(35) Dunning, F. B.; Stebbings, R. F. *Annu. Rev. Phys. Chem.* **1982**, *33*, 173−189.
(36) Kalamarides, A.; Walter, C. W.; Lindsay, B. G.; Smith, K. A.; Dunning, F. B. *J. Chem. Phys.* **1989**, *91*, 4411−4413.

Oppenheimer approximation is no longer valid.[37,38] The positive alkali core ion can strongly interact with the transient molecular anion, and in some experiments "bond stretching" is observed in the acceptor during the electron transfer.[37−39] This interaction can produce different negative ions from those obtained by attachment of free electrons.[22,40] Thus, the parent negative ion is observed here because the positive core interacts with the nascent molecular ion to make the stable region of the $^2B_1$ state available in a nonvertical transition. As discovered in previous experiments with oriented molecules, the electron enters a low-lying unoccupied MO,[25,41] rather than simply attaching to the positive end of the dipole. The present experiments show also that the electron-transfer collision can itself alter the nature of the LUMO by distorting the nuclear geometry.

Do these experiments probe the dipole bound (DB) negative ion? Apparently not. The inherent nature of the electron-transfer processes observed here inhibit the formation of DB ions because their formation requires a donor with a comparably diffuse orbital satisfied by high-lying Rydberg atoms with $n \approx 15$,[13,15,16] whereas $n = 3$ for sodium. If DB $CH_3NO_2^-$ ions were made in the present experiments, they would survive our electric fields of 300 V/cm, far less than the ~15 kV/cm[16] required for field detachment, reach the detector, and be counted as parent negative ions. The ions observed at the lowest energies have the greatest likelihood of being DB, but the electron density should be broadly centered about the positive end of the dipole, as suggested by the LUMO in neutral geometry, Figure 9c. Electron transfer would thus be strongly favored for attack at the CH_3 end of the molecule, but this is not observed, suggesting these are not DB ions. The parent $CH_3NO_2^-$ ion is still observed at collision energies several eV above threshold, inconsistent with formation of a fragile DB ion. We finally note that CH_3CN ($\mu = 3.92$) has a well-characterized DB ion, but in similar experiments, we do *not* see parent negative ions or free electrons from CH_3CN.[23] It is thus highly unlikely that a fragile DB ion is formed in these experiments. The interaction between the nascent negative and positive ion perturbs the geometry of the molecule, making valence-bound orbitals available. Thus, it appears that, although a dipole-bound ion could evolve to a valence-bound state and thereby be a doorway state, formation of the valence-bound state does not require a DB precursor.

V. Summary

We have studied electron-transfer collisions between sodium atoms and oriented CH_3NO_2 molecules to probe the spatial extent of the molecular LUMOs. Positive and negative ions are detected in coincidence for attack at both the CH_3-end of the molecule and the NO_2-end. The energies studied are a few eV above the threshold for ion-pair formation (~4.9 eV). The major negative ions are the parent ion, $CH_3NO_2^-$, NO_2^-, O^-, and the free electron. CN^- has been previously reported, but we conclude that this ion does not arise from CH_3NO_2 monomer.

The steric asymmetry for formation of e^- and NO_2^- seems to be zero, consistent with sideways attack at a π^*_{NO} orbital, and inconsistent with electron transfer to a σ^*_{CN} orbital. These species seem to arise from the same precursor because the electron fraction maximizes at energies close to the threshold for formation of NO_2^-. We believe this precursor is a vibrationally excited $CH_3NO_2^-$ ion in the $^2B_1$ state corresponding to the occupation of the π^*_{NO} orbital. A curve crossing between the $^2B_1$ (π^*_{NO}) state and the $^2A_1$ (σ^*_{CN}) state is apparently responsible for transferring electron density from the π^*_{NO} orbital into the σ^*_{CN} orbital so that the C−N bond can be broken. Some evidence suggests that the crossing occurs with an activation energy ~0.4 eV.

Methyl-end attack weakly favors the parent negative ion, $CH_3NO_2^-$ near the threshold, and NO_2 end attack favors formation of O^- at energies ~2 eV above threshold. Although methyl-end attack would be favored for formation of a dipole-bound negative ion, the strong interaction between the positive alkali core and the transient negative ion makes formation of a valence-bound ion more likely. Formation of salt molecules, $NaNO_2$, is increasingly favored at low energies, in orientations where the Na^+ ion is nearer the NO_2. Salt formation would thus account for a slight diminution of signal at the NO_2-end, leaving a weak preference for methyl-end attack to form the parent ion.

Acknowledgment. We gratefully acknowledge support received for this work from the Robert A. Welch Foundation and the National Science Foundation. Acknowledgment is made to the Donors of the American Chemical Society Petroleum Research Fund for partial support of this research. C.R. thanks the Ford Foundation for a Predoctoral Fellowship. We thank Jacques Normand for his help with the Gaussian calculations and Terry Kennair for his assistance in the laboratory.

Supporting Information Available: Complete citation for ref 33. This material is available free of charge via the Internet at http://pubs.acs.org.

JA058206T

(37) Kleyn, A. W.; Los, J.; Gislason, E. A. *Phys. Rep.* **1982**, *90*, 1−71.
(38) Kleyn, A. W.; Moutinho, A. M. C. *J. Phys. B: At. Mol. Opt. Phys.* **2001**, *34*, R1−R44.
(39) Hubers, M. M.; Kleyn, A. W.; Los, J. *Chem. Phys.* **1976**, *17*, 303−325.
(40) Aten, J. A.; Los, J. *Chem. Phys.* **1977**, *25*, 47−54.
(41) Jia, B.; Laib, J.; Lobo, R. F. M.; Brooks, P. R. *J. Am. Chem. Soc.* **2002**, *124*, 13896−13902.